Eng. Sci., 2022, **19**, 330–342

Engineered Science

DOI: https://dx.doi.org/10.30919/es8e732

Analytical and Computational Investigation of Blood Flow in Generic Aortic Aneurysm: A Closed Conduit Approach

Sunitha Lasrado,[1,#] R Vinoth[1,#,*] and S Balaji,[2,#]

Abstract

An abdominal aortic aneurysm (AAA) is a potentially fatal cardiovascular condition defined by a focal dilation of the blood vessel. AAA rupture is not only caused by biological factors but also by mechanical parameters of the aortic wall. This work designs generic aneurysms and performs analytical and computational investigations. The objective of the investigation is to examine Wall shear stress (WSS), velocity, and aortic pressure, factors that affect the aorta wall's integrity. The fluid flow in AAA models was studied using computational fluid dynamics (CFD) to examine the effects of geometrical features and boundary conditions. The study focuses on the steady-state behavior of aortic aneurysm models with Reynolds numbers ranging from 500 to 7500. The generic aorta designs showed a deviation of 2% in the pressure difference and 4% in the WSS. Subsequently, the maximum velocity deviated by 0.7% from the theoretical value in the design. The aneurysmal aorta model with gradual expansion and contraction showed pressure uncertainty of 2% and a velocity variation of about 3% based on analytical and CFD results. These results relate to how close the theoretical and computational outcomes match and help comprehend the aortic aneurysm's disease under laminar and turbulent flow conditions.

Keywords: Computational fluid dynamics (CFD); Aneurysm; WSS; Pressure; AAA; Wall properties; Laminar; Turbulence.
Received: 03 April 2022; Revised: 31 May 2022; Accepted: 03 June 2022.
Article type: Research article.

1. Introduction

There is an ongoing interest in predicting and preventing cardiovascular system diseases in medicine. This motivation drives the study of cardiovascular system blood flow dynamics, referred to as cardiovascular hemodynamics. An aortic aneurysm (AA) is a multifactorial aneurysm with high mortality associated with old age.[1-3] It is more prevalent in men than women, with abdominal aortic aneurysms (AAA) claiming 200,000 lives worldwide each year.[4,5] There is no definite approach to assessing the risk of AAA rupture rather than the limited AAA-size clinical guidelines.[6] An AAA is ruptured when the integrity of the aortic wall is lost, resulting in a balloon-like bulge. Thus, an aneurysm is a constricted, disorderly section of an artery prone to rupture. The term AAA refers to a dilatation of the abdominal aortic aneurysm that is more than 1.5 times that of the neighboring healthy vessel.[7] Before rupture, most patients with AAAs are asymptomatic; effective screening and evaluation methods are critical for accurate AAA detection and behavior.[4] The diameter measurement is considered the medical criterion for determining aneurysm rupture.[8] More than the diameter of the aneurysm, biomechanics play a crucial role in AAA rupture. Apart from biological factors, AAA rupture is also a result of mechanical parameters that constantly affect the wall tissue due to its abnormal value. Evaluating these parameters could significantly improve patient care.[9] The disease progresses more quickly by reducing blood flow in AAA.[10] A precise prediction of AAA growth and rupture risk is a challenging problem attracting much attention. Aortic wall shear stress, pressure, and velocity are some of the mechanical factors that affect the biomechanics of AAA rupture.[11] The hemodynamic stresses are crucial as they drive the growth and breakdown of AAA. The aneurysm to aorta ratio is used in the prediction of high-risk aneurysms. This is because patients with ratios greater than 2.7 are more likely to develop symptoms, whereas those with ratios greater than 3.4 are more likely to rupture.[12] Thus, in laminar cases, the effect of wall shear stress (WSS) and pressure is proportional to the strength in the wall of the aneurysm aorta model.[13] Their study found a strong

[1] *Dept. of Electronics and Communication, Manipal Institute of Technology, Manipal Academy of Higher Education, Manipal 576104, Karnataka, India.*
[2] *Dept. of Biotechnology, Manipal Institute of Technology, Manipal Academy of Higher Education, Manipal 576104, Karnataka, India.*
**Email:* vinoth.nair@manipal.edu (R Vinoth)
[#] *These authors contributed to this work equally.*

correlation between an aneurysm rupture and WSS. The highest peak is attained at a maximum magnitude roughly twice the tube entrance. Slow turbulence in the entrance tube is greatly magnified in intensity and length as it finds its way into the aneurysm. Stress on the artery wall is used to estimate rupture risk more precisely than just looking at the diameter of the vessel.[14]

WSS peak values and wall stress are typically considered the footprints of failure in an aneurysm.[6] Their study aimed to ultimately get a clinically helpful tool to decide whether the repair is necessary or not. The studies explored generic AAA models using CFD and investigated the effect of different parameters on blood flow.[15] From the literature, the study across the last two decades showed that computational software for fluid engineering used for biomechanics has wholly revolutionized CFD development. CFD studies employ mathematical models. They are applied to simulate conditions for blood flow, vessel forms, aneurysms, velocity, and stress forces such as stress or tension.

Design of Experiments (DOE) of the Computer-Aided Design (CAD)generated geometries yielded correlations between geometry and maximum stress in the arterial wall.[16] They aimed at providing clinicians guide to the initial diagnosis of AAA in geometry, allowing indices other than the maximum diameter to predict the risk of rupture. Related studies used Color Doppler flow imaging (CDFI) and Laser-Doppler Anemometry (LDV) for pressure and wall shear stress measurements.[17,18] They found that variations in the Reynolds number significantly affected steady flow in an AAA model. The nature of the flow, whether turbulent or laminar, is determined by the Reynolds number. If the Reynolds number is less than 2300, the flow is laminar, and if it is more significant than 4000, it is turbulent. The Reynolds number is a standard method for determining the blood flow model.[19] Reynolds number is used to determine the fully developed profile length. An approximate value of $0.0625R_e$ was found in Applied Hydro and Aerodynamics for the length (L) to diameter (D) ratio for laminar flow.[20] Furthermore, in the literature, various equations for developing length are presented. The developed entry length for laminar flow is $L_{(\text{laminar})} = 0.05\ R_eD$, and Turbulent flow is specified by $L_{(\text{turbulent})} = 1.359\ DR_e^{1/4}$, where D is the diameter of the pipe, R_e Reynolds number and $L_{(laminar)}$ the length of the entry pipe.[21] Another equation for turbulent flow is given by $L_{(\text{turbulent})} = 4.4\ DR_e^{1/6}$.[22] Closed conduits are the only cases in which these equations can be used. The literature shows a significant association between the Reynolds number and the growing length of laminar flow. It is not the case in a turbulent flow. As shear stress has less opportunity to interact with a fluid in turbulent flow, the developing length is smaller than the laminar flow. As a result, it can be concluded that shear stress at the wall is more critical in laminar flow than in turbulent flow.[23] Another mechanical factor of importance in predicting the rupture in an aneurysm is blood pressure. It is the force exerted by flowing blood against the artery walls. The human heart's pumping action generates pressure waves. Blood pressure tends to rise in many cases due to numerous abnormalities. Thus, simulation studies of pressure waves in the human system play a critical role in diagnosing the affected area of the human body.[19]

The wall pressure is the kinetic energy of the blood transported perpendicular to the vessel surface as an inertial force. In disparity, the wall tension is the force exerted by the wall in an equal magnitude and opposite direction to the wall pressure. The aneurysm ruptures if the wall tension is larger than the wall's tensile strength.[24] Depending on the velocity and viscosity of the blood, WSS can increase. Hydrostatic pressure and WSS distribution may play a vital role in the growth of AAA aneurysms.

Researchers have related WSS variations in different viscous scenarios. They believed that the differences between Newtonian and non-Newtonian models are insufficient to justify the presumably more significant numerical effort required to calculate non-Newtonian viscosity variations. Research continues in this direction, as the distinction between Newtonian and non-Newtonian mechanics is not entirely clear.[25] They studied how non-Newtonian features have impacted velocity fields. Their study found that the concept of Newtonian and non-Newtonian blood flow parameters significantly affects flow patterns within an aneurysm and shear stress on the AAA wall. For a specific study, researchers were interested in finding out how well each of the three turbulent models predicted flow outlines, velocity profiles, and turbulence concentration profiles in a pipe with rapid expansion and turbulent diesel flow. The merits and disadvantages of each model were analyzed.[26]

The literature review found a necessity to understand the biomechanical parameters leading to Aortic rupture. Aneurysm dilations and the need to examine aneurysm ruptures are studied in depth. The probability of occurrence of an aneurysm needs to be understood. As a result, research is conducted to investigate the biomechanical relationships between stress, strength, and rupture risk. This study explores the effects of fluid fluctuations in aneurysms in general. Generic models are more flexible and are applied to a broader range of situations. A thorough explanation of the issue that allows for a more accurate comparison is done. This study evaluated the effect of geometric parameters on flow patterns with pressure distribution in AAA models combined with boundary conditions using CFD.

Furthermore, the effect of boundary conditions on the flow patterns of these geometric variations was critical to comprehend. Literature gave an insight into how the WSS estimator can be used to predict AAA. The rupture of AAA was addressed by studying the wall pressure also. Hemodynamic pressure variations, velocity, and wall shear stress distributions are evaluated from flow patterns. The complete characteristics of the laminar flow fields are studied to determine the onset of turbulence. The current work considered non-Newtonian, rigid, steady-state, and generic

models. The purpose of doing linear stability assessments on flows is to understand better the mechanisms underlying the start of instability, which would aid in knowing the flow behavior in more complicated flows. This work considers smooth expansion and contraction for the design of the aneurysmal aorta model.

2. Numerical Analysis

This section reveals the flow parameters and structure of the generic and aneurysmal aorta model. It considers the study of developed profiles and their importance in this study.

2.1 Problem Definition and Mathematical Requirement

A fully developed profile was created using the specifications given in Table 1. The Reynolds number describes the dilation length, the maximum diameter, and the physical flow parameters, which characterize the problem accordingly. According to the literature studied, fully developed equations[27] marked the starting point for this work. The fully developed profile Equations (1) and (2).

$$L_e = 0.06 R_e d \quad (1)$$

$$R_e = \frac{\rho V_{avg} d}{\mu} \quad (2)$$

Table 1. Design considerations for a fully developed profile.[28,29]

Variable	Description	Value
L_e	entrance length	1.83 m
R_e	Reynolds number	1170
ρ	density	1050 kg/m^3
μ	viscosity	3.5*10^{-3} Pa
V_{avg}	Average velocity	0.15 m/s
d	diameter	0.026 m

The fully developed profile generated is illustrated in Fig. 1. It refers to the analytical and CFD results of the fully developed profile. It is seen that the analytical and CFD results got from the simulation nearly overlap with each other, indicating the matching of these results graphically.

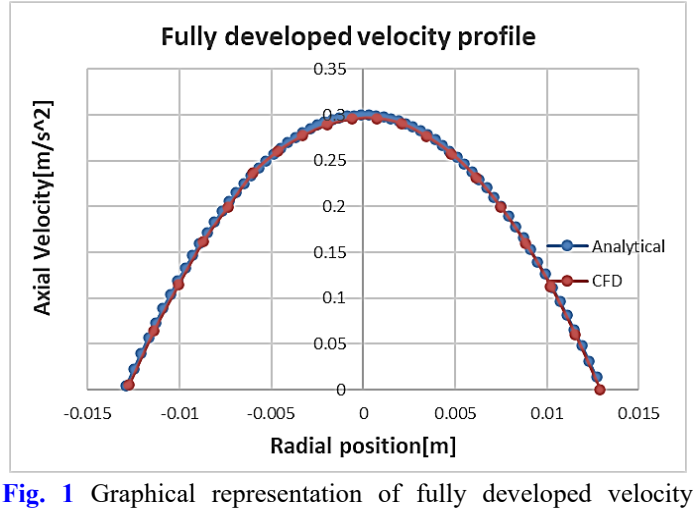

Fig. 1 Graphical representation of fully developed velocity profile.

This developed profile is fed into both the aneurysmal and generic aorta models. The fully developed profile was designed using the ANSYS Design modeler,[30] and the settings of boundary conditions like non-Newtonian, rigid, and Incompressible were considered and designed using ANSYS CFX (v15.0, ANSYS, Canonsburg, PA, USA) software.[31] Figs. 2(a) and 2(b) show the developed profile, respectively. This developed profile seen acts as an input to the actual measurements of the generic and aneurysm model designs.

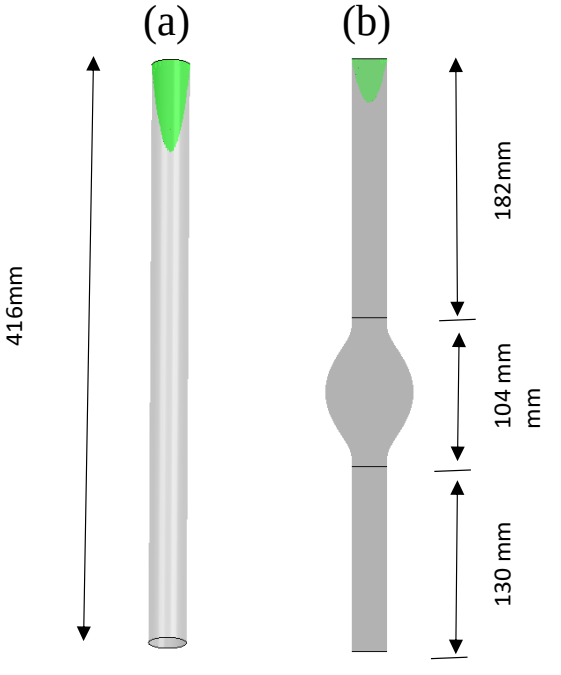

Fig. 2 Developed profile as input to (a) generic aorta model and (b) Aneurysmal aorta model.

This generic design was extracted from the literature.[17,18,32,33] is designed and shown in Fig. 3. The parameters considered in the design are from.[27,28] The human aorta has a complicated shape that varies according to the patient. Its structure and shape are highly varied among people. This study aims to create computational methods for determining the ground truth for a simple, generalized abdominal aortic aneurysm. As a result, the shape of a generic aneurysm model based on Bauer's[28] work is employed. The model aneurysms explored here are axisymmetric, with Gaussian-shaped wall inflation. This shape has a benefit over the sinusoidal forms employed in previous research.[34] Its spatial derivatives are continuous to all orders - a desired property, particularly for hydrodynamic stability studies; also, it is what one would anticipate in true aneurysms.[35] Equation (3) provides the length L for the generic aorta model considered in the design.

$$L = 16\, d \quad (3)$$

Figure 4 depicts a fusiform aneurysmal geometry in two dimensions. To be expressed as Equation (4) that varies with diameter D, the aneurysmal wall's smooth expansion and contraction sections are from Equation 1.[28]

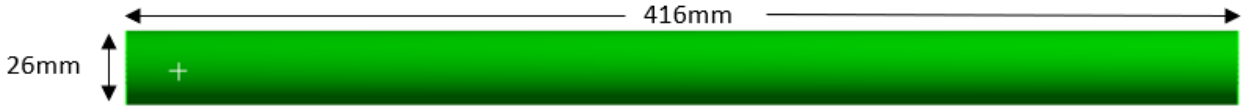

Fig. 3 Un-dilated generic aorta model design.

$$r_A\left(\frac{x}{d}\right) = \frac{1}{2} + \frac{\alpha-1}{2}\, exp\left(4^{\gamma} - \left(0.25 - \left(\frac{(x/d)+2}{4} - 0.5\right)^2\right)^{-\gamma}\right) \quad (4)$$

where γ = 0.7186. Consider a steady flow in a straight tube with the bulge as indicated in Fig. 4 in vitro AAA model. The aneurysm radius r_A is a function dependent on dimensionless length x/d € [-2,2], where x is dependent on the axial distance measured from the point of maximum diameter. The maximum diameter expansion is α = D/d = 2.5, D is the dilated diameter, and d is the un-dilated diameter for the entire design. The aneurysm length L = 104 mm. The ratio of aneurysm length to un-dilated diameter is L/d, equating to 4. Table 2. depicts the models designed with the aspect ratio α given by D/d.

Table 2. Specifications used for the design of Aneurysmal aorta models.

Model number	L/d	α = D/d
1	4.0	1.25
2	4.0	1.5
3	4.0	1.75
4	4.0	2
5	4.0	2.5

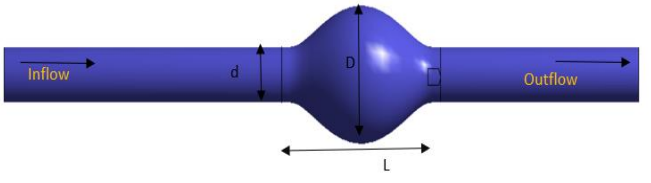

Fig. 4 Model 5 design with dimensions used for numerical and analytical analysis.

The mean axial velocity considered for the design is 0.15m/s, and thus the Reynolds number is deduced to 1170 accordingly. For the bulge diameter to vary according to the aspect ratio α, Equation (4) is considered. The values deduced from the equation generate different curves for different aspect ratios, as shown in Fig. 5. An ANSYS Inc., Canonsburg, PA[30,31] Design modeler feeds these generated curves. Model 5, shown in Fig. 5, was designed similarly to the generic aorta model with aneurysm dimensions varying concerning x/d. According to the design, the aneurysm length varies from 0 to 4d; the aneurysm length L tends to be 104mm. According to the literature, the author considered a predecessor of 2d at the pipe intake.[28]

The mesh designs were achieved using commercial software from ANSYS mesh to discretize the domain and are seen in Figs. 6(a) and 6(b), respectively. According to,[28] quadrilateral cells are used in a way so that these cells can be easily stretched to account for different flow gradients in various flow directions. The different bulge size variations are realized in Figs. 7(a-e).

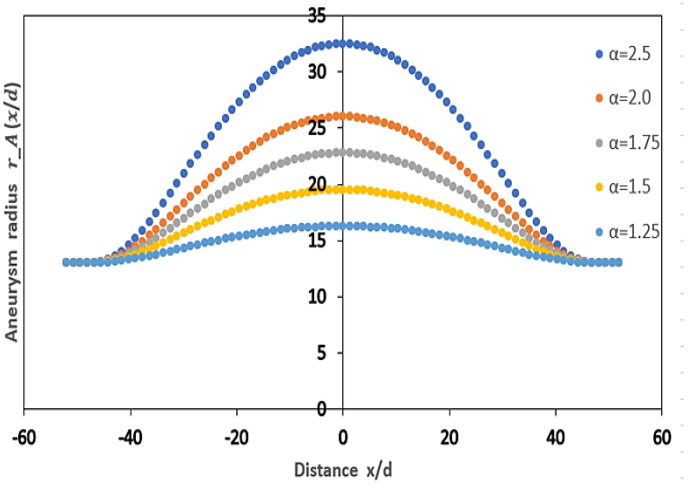

Fig. 5 Input waveforms generated for different aneurysm values.

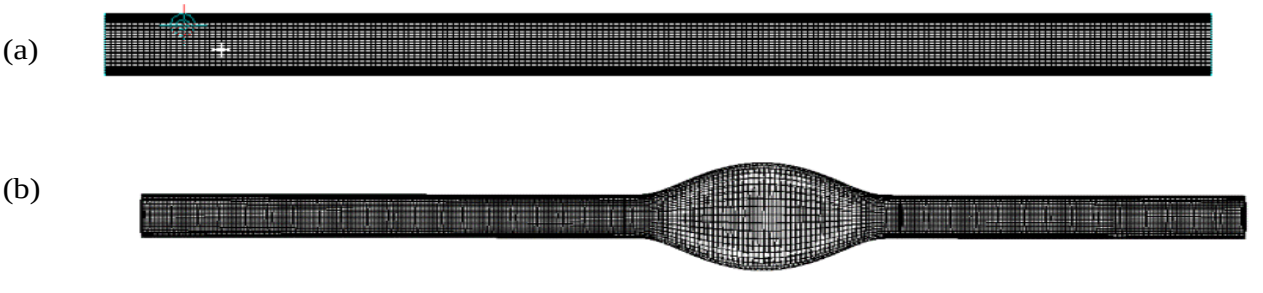

Fig. 6 Grid generated by computational dynamics (a) non-dilated generic aorta model (b) Dilated aneurysmal aorta model.

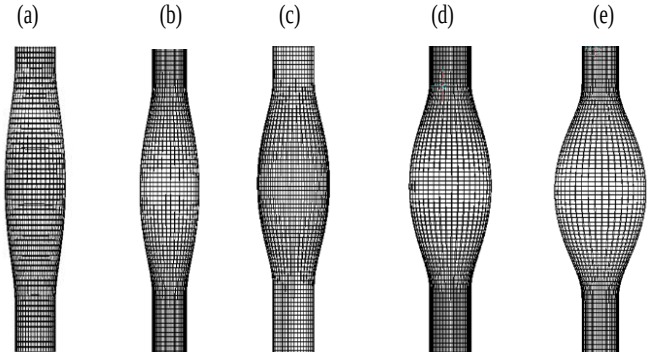

Fig. 7 Mesh generated for different aneurysmal aorta models.

2.2 Flow physics, Parameters, and Boundary Conditions

The incompressible fluid was employed for the design simulation with CFD, and the flow-related equations were considered. In the research, there were several critical considerations to be made. Blood considered in this study was non-Newtonian fluid. Blood was modeled as having a density ρ of 1050 kg/m^3. The design employed a dynamic viscosity μ of 0.0035 Pa·s.[29,36-39] papers referred to the values considered in the design. These values were used across all designs and are believed to meet the design's specific requirements. For the entire design, the inlet velocity was set to v = 0.15 m/s.

The equations governing the fluid flow for incompressible non-Newtonian fluids are equations of continuity and Navier-Stokes. The continuity equation is represented in vector notation by Equation (5) given by 2.4.[40]

$$\frac{\partial \rho}{\partial t} + div(\rho\mu) = 0 \tag{5}$$

where $\frac{\partial \rho}{\partial t}$ is the change in density, and div(ρu) is the net flow of mass across boundaries that is a convective term where $div = \hat{\imath}\frac{\partial}{\partial x} + \hat{\jmath}\frac{\partial}{\partial y} + \hat{k}\frac{\partial}{\partial z}$ and $u = \hat{\imath}u + \hat{\jmath}v + \hat{k}w$. Equations (6), (7), and (8) refer to the Navier stokes equations in the x, y, and z directions.[40-43]

$$\rho\frac{Du}{Dt} = -\frac{\partial p}{\partial x} + \frac{\partial \tau_{xx}}{\partial x} + \frac{\partial \tau_{yx}}{\partial y} + \frac{\partial \tau_{zx}}{\partial z} + S_{M_x} \tag{6}$$

$$\rho\frac{Dv}{Dt} = -\frac{\partial p}{\partial y} + \frac{\partial \tau_{xy}}{\partial x} + \frac{\partial \tau_{yy}}{\partial y} + \frac{\partial \tau_{zy}}{\partial z} + S_{M_y} \tag{7}$$

$$\rho\frac{Dw}{Dt} = -\frac{\partial p}{\partial z} + \frac{\partial \tau_{xz}}{\partial x} + \frac{\partial \tau_{yz}}{\partial y} + \frac{\partial \tau_{zz}}{\partial z} + S_{M_y} \tag{8}$$

S_{M_x}, S_{M_y}, S_{M_z} The body and surface forces contribute to pressure and viscous or shear stresses. Navier-Stokes equations are used for determining flux fields within a specimen geometry. Most CFD solvers are engineered to use these equations in their solvers. The Navier-Stokes equations, also termed conservation of momentum and energy equations, are the fundamental equations that govern motion and conserve mass and energy. These equations are solved at each nodal point for a mesh produced in CFD geometry.

2.3 Analytical Pressure Calculations for the Generic aorta model

Equation (9) gives analytical differential pressure calculations, taken from 8.21.[27,44]

$$\Delta P = \frac{L\rho\Lambda V_{avg}^2}{2d} \tag{9}$$

ΔP represents the pressure difference between the inlet and the outlet. Equation (10) represents Wall shear stress τ given.[27]

$$\tau = \frac{d\Delta P}{4L} \tag{10}$$

2.4 Analytical Pressure Calculations for the Aneurysmal aorta model

Equation (11) gives the inlet velocity profile generated for the aneurysmal aorta model.[44]

$$u(r) = 2 * V_{avg}[1 - \left(\frac{r}{R}\right)^2] \tag{11}$$

The pressure value considered from[45,46] is given in Equation (12)

$$\Delta p = \Delta p_1 + \Delta p_2 + \Delta p_3 + \Delta p_C + \Delta p_E \tag{12}$$

where Δp_1, Δp_2 and Δp_3 are the pressure in the proximal region of the aneurysmal aorta model, the drop in pressure in the aneurysm region, and the drop in pressure at the model's distal region, respectively. Δp_C, contraction pressure, at the aneurysm inlet and Δp_E expansion pressure at aneurysm outlet. Δp_1, Δp_2 and Δp_3 are calculated according to Equation (13)[44] Δp_C and Δp_E . They are calculated according to Equations (14), (15), and (16)[27]

$$\Delta P = \frac{L\gamma\rho V_{avg}^2}{2d} \tag{13}$$

$$\Delta p_C = h_C * \rho * g \tag{14}$$

$$\Delta p_E = h_E * \rho * g \tag{15}$$

$$\text{where } h_C = h_E = K\frac{V_{avg}^2}{2*g} \tag{16}$$

where in this design, the K value considered is for a smooth contraction and smooth expansion pipe.[47]

3. Results and Discussions

This section summarizes the main findings of the work. At the outset of this work, generic aorta without aneurysm and aneurysmal aorta models were designed. Analytical checks were made on WSS, pressure, and velocity parameters, and the results were recorded. Similarly, CFD simulations were performed on the design. Theoretical and computational fluid dynamics (CFD) results were compared. There were variances in pressure ΔP, WSS, and velocity that were found in the literature studied. Laminar models with Re numbers 1170 and 1800 were studied in this research. WSS and pressure variations were explored as a result. For 5000 and 7500 Re numbers, turbulence models were created. These turbulent simulations had a distinct effect on the WSS, pressure, and velocity. Furthermore, three turbulent models, namely SST, K-ϵ, and RNG K-ϵ, were simulated. The results of these simulations were used to investigate biomechanical parameters affecting the vessel wall of the arteries

Figure 8 shows the conditions for the upstream flow before the bulge of the AAA (Model 5). The general flow

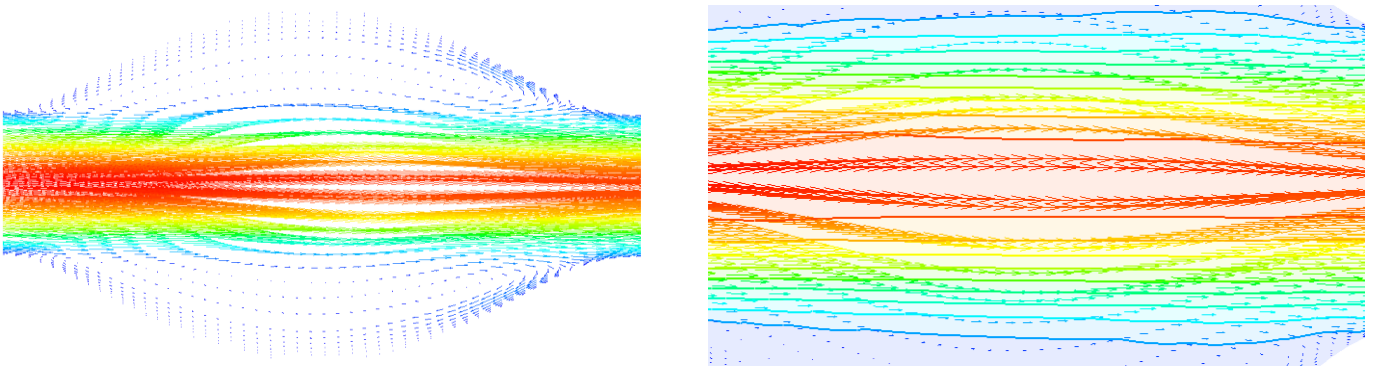

(a) (b)

Fig. 8 Velocity vector plots (a) Model 5 and (b) generic aorta model, under steady flow condition, Re number 1170.

characteristic in the bulge was mainly a fluid jet, flanked on both sides by weak vortices of the recirculation type. The flow recirculation was caused by the negative pressure gradient forced on the bulge as the cross-section area increased. The flow properties did not change considerably when the bulge size was reduced (Model 1). This finding is identical.[13]

As can be seen, the velocity vector in the bulge's center has the most significant velocity compared to the velocity vectors at the walls. This is because the wall is rigid, and the flow is held in contact with the wall.

Figure 9 shows that the CFD results coincide with the values obtained through analytical calculations, indicating that the simulation results are comparable to that obtained through the plotting of the waveform according to Equation (11). Furthermore, an analysis of the aneurysmal aorta model with different aneurysm ratios of α was carried out for different laminar and turbulent conditions.

The analytical values for the generic aorta without aneurysm and Aneurysmal aortic design are represented in Tables 3 and 4, respectively.

The CFD results of the generic aorta model through the simulation are tabulated in Table 5. These CFD results were compared with the analytical results calculated through the equations and tabulated in Table 3. The CFD results observed in Table 5 showed that the maximum velocity matches the theoretical value with a 0.7% deviation. The difference in pressure ΔP and the WSS matched with mesh elements of 104800 elements when the analytical and theoretical calculations were performed. A 2% variation in the pressure difference and 4% in the WSS was seen for a generic aorta model design.

Table 3. Analytical calculations of Generic aorta model design.

ΔP [Pa]	Max_Val Velocity Outlet [m s^-1]	maxwallshear [Pa]
10.33846	0.3	0.161538

The analytical and CFD results for the aneurysmal aorta model were observed. The difference between the calculated drop in pressure and the actual drop in pressure can be defined as uncertainty. In the design of the aneurysmal aorta model, smooth transitions at the expansion side and the contraction side were considered according to the design.[47] The Analytical results were calculated through the equations and tabulated in Table 4. The CFD results observed in Table 6 show that the maximum velocity matches the theoretical value

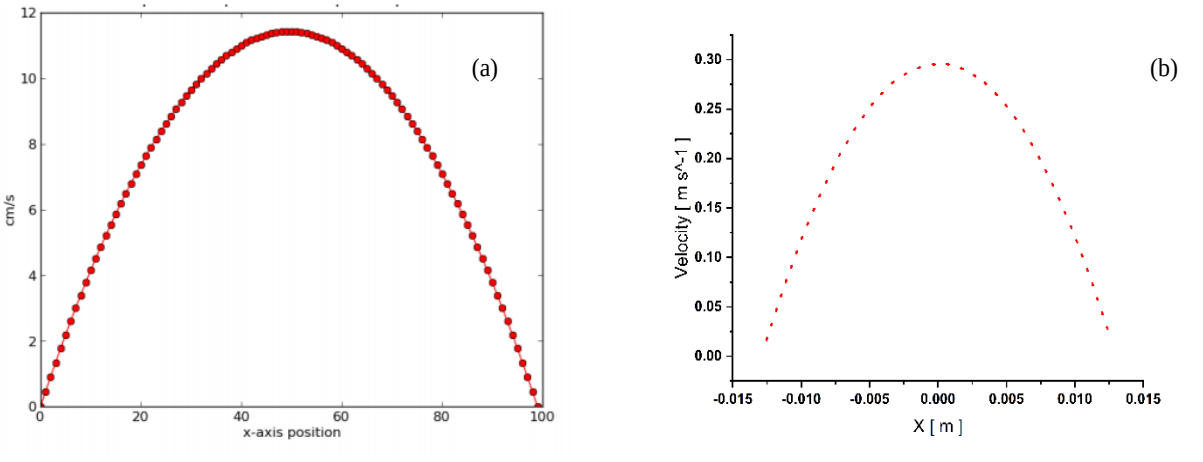

Fig. 9 Velocity profile in a generic aorta model flow (a) Theoretical graph (b) Simulated graph.

Table 4. Analytical calculations for generic aneurysmal aorta model design.

ANEURYSM SIZE RATIO $\alpha = \frac{D}{d}$	DILATED DIAMETER (MM) D	Δp_1 (PROXIMAL REGION) (7D) (PA)	Δp_2 (ANEURYSM REGION) (4D) (PA)	Δp_3 (DISTAL REGION) (5D) (PA)	PRESSURE DUE TO EXPANSION Δp_E = h_E*G*P (PA)	PRESSURE DUE TO CONTRACTION Δp_C = h_C*G*P (PA)	TOTAL PRESSURE $\Delta P = \Delta p_1 + \Delta p_2 + \Delta p_3 + \Delta p_C + \Delta p_E$ (PA)	WALL SHEAR STRESS T = $(D * \Delta P)/(4*l)$ (PA)
1.25	0.0325	4.5230	2.067692	3.230769	0.23625	0.23625	10.2940385	0.160671823
1.5	0.039	4.5230	1.723076	3.230769	0.23625	0.23625	9.94942308	0.192805988
1.75	0.0455	4.5230	1.476923	3.230769	0.23625	0.23625	9.70326923	0.224940153
2	0.052	4.5230	1.292307	3.230769	0.23625	0.23625	9.51865385	0.257074317
2.5	0.065	4.5230	1.033846	3.230769	0.23625	0.23625	9.26019231	0.321342647

Table 5. CFD results in the generic aorta model.

Mesh Sizing(mm)	Mesh Elements	Pressure Difference ΔP [Pa]	max ValVelocity Outlet [ms^-1]	maxwallshear [Pa]
5	99800	9.79526	0.29710	0.16110
4	104800	10.0948	0.29789	0.16808
3	113600	9.75895	0.29804	0.16753
2.5	1230	9.84242	0.29639	0.16273
2	138000	10.0217	0.29870	0.17779
1.5	156800	10.1307	0.29814	0.17736

Table 6. CFD Results of the aneurysmal aorta model.

Aneurysm size ratio	Mesh Elements	ΔP [Pa]	maximal Velocity Outlet [m s^-1]	Max wall shear [Pa]	Average wall pressure (Pa)
1.25	131286	9.9923	0.297	0.206	9.813
1.5	132496	10.021	0.297	0.303	9.8841
1.75	133133	10.062	0.297	0.324	9.88
2	133770	10.1	0.297	0.342	9.918
2.5	135680	10.216	0.297	0.375	10.003

with a 3% deviation. It is also seen that the pressure uncertainty got from Analytical and CFD results is 2%, and uncertainty of 10% can be accepted due to smooth transitions and expansion of the generic pipe.[47] In the case of a smaller aneurysm, WSS is also reduced. WSS increases as the bulge size increases. Hence WSS is one of the criteria that needs to be taken care of in an abdominal aortic aneurysm.

This section analyses the principal flow and conclusions for steady-state through the bulge model, particularly AAA. Specifically, the changes in flow parameters as the increasing bulge are explored. Fig. 10 shows that for various ratios of aneurysm bulge, the wall shear distribution at the distal side of the aneurysm is higher than the proximal. The WSS is also seen to be minimal at the bulge. Observations indicate that as the dilated diameter grows, the WSS reduces at the proximal end and increases at the distal end. Wall shear pressures during inflation are minimal compared to straight vessels. Several

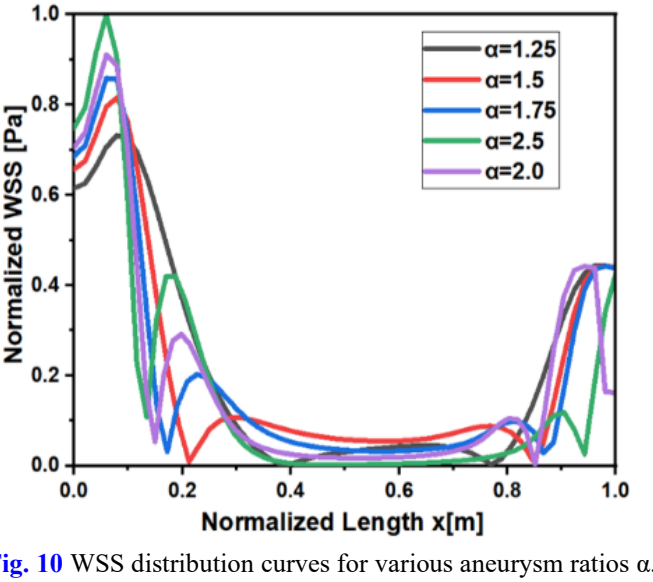

Fig. 10 WSS distribution curves for various aneurysm ratios α.

pressure curves are plotted against various bulges of the aneurysm, as depicted in Fig. 11. The bulge's midpoint provides the bulge's maximum apparent pressure at all flow rates.

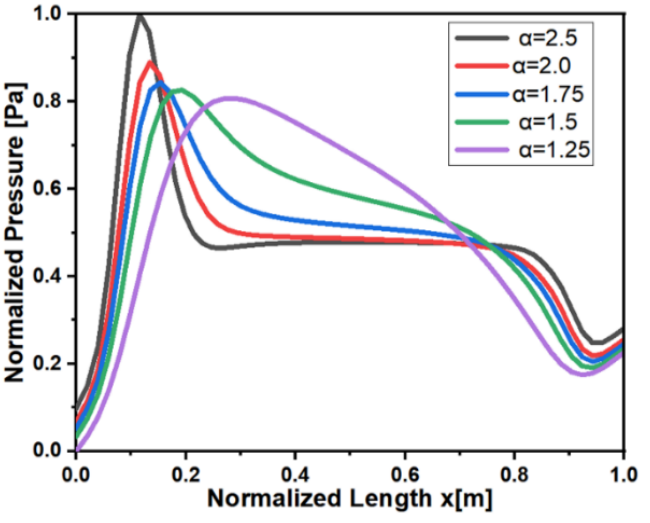

Fig. 11 Pressure distribution curves for various aneurysm ratios α.

Figure 12 shows the velocity profiles at different bulge points related to the maximum velocity at the output at various bulge points. It is observed in Fig. 13. There is no recirculation region when the bulge is 1.25 times lesser than the inlet. The recirculation region increases as the corresponding bulge region expand. The dynamics of both pressure and the shear stress distribution in this region, as well as the effect of flow-induced stress on the potential of the aneurysm, are studied in detail.

First, the steady-state dynamics of a cardiovascular system segment were simulated. The steady analyses help understand the time-averaged dynamics of streams in the region of interest and identify specific regions prone to extreme WSS and spatial variations. Besides, the study included Reynolds numbers 1170 and 1800, which were both laminar cases, and turbulent flow conditions were investigated with Reynolds numbers 5000 and 7500, which depended on the diameter and average velocity. Compared to the SST turbulent value, which tends to the highest point of the normalized value of 1Pa at the distal end, the normalized values for wall shear stress fell below 0.1Pa for laminar cases. As seen from the graphs shown in Figs. 14a-e, an observation is made where the WSS is as low as 0.1

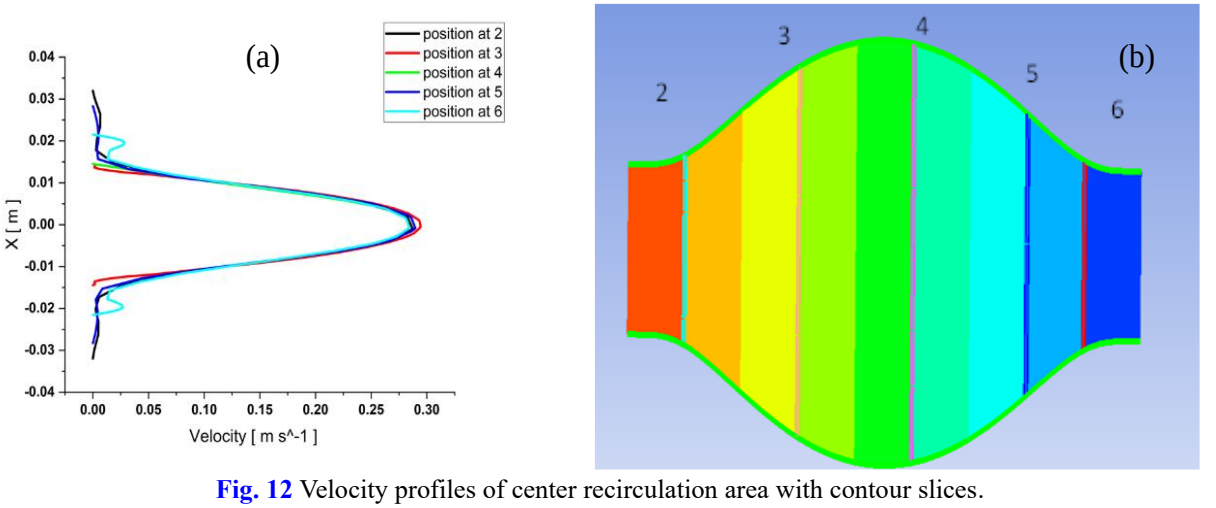

Fig. 12 Velocity profiles of center recirculation area with contour slices.

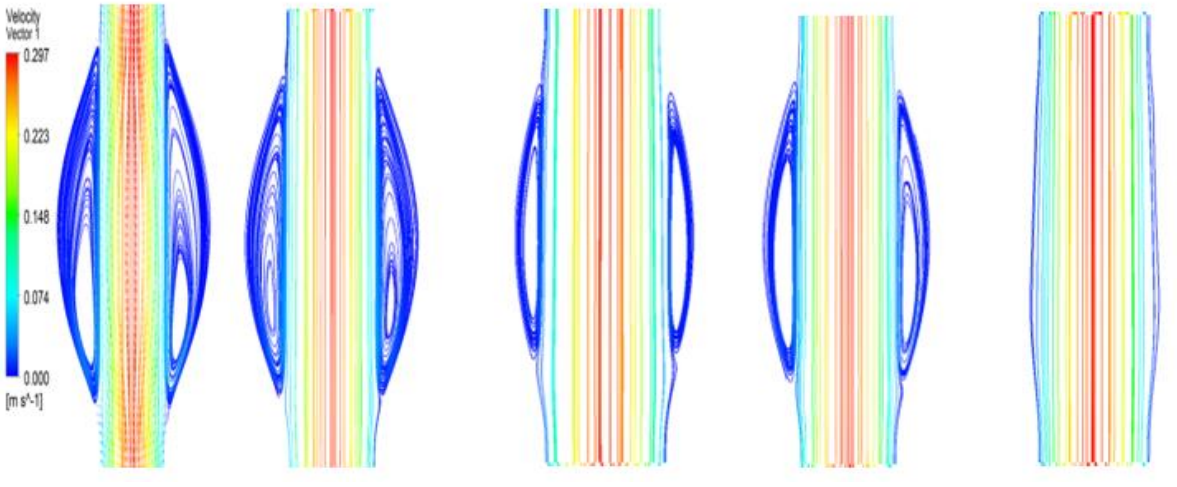

Fig. 13 Streamlines past the aneurysms in the aneurysmal region with various grades of radial expansion (a) α = 2.5 (b) α = 2.0 (c) α = 1.75 (d) α = 1.5 (e) α = 1.25.

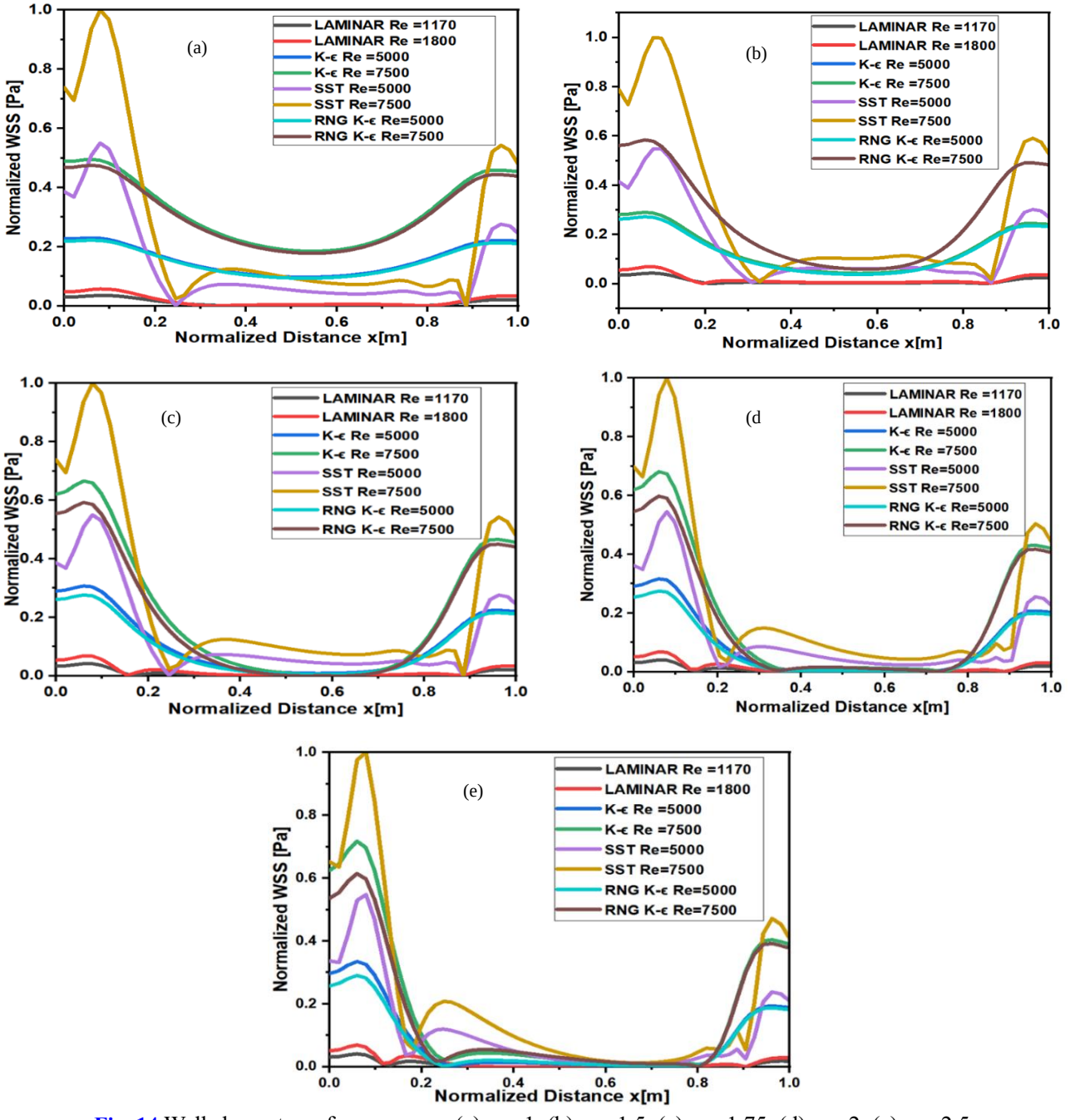

Fig. 14 Wall shear stress for aneurysm (a) α = 1, (b) α = 1.5, (c) α = 1.75, (d) α = 2, (e) α = 2.5.

Pa for all ranges of bulges α = 2.5 to α = 1.25. In the case of laminar conditions at the proximal and distal regions of the aneurysms, WSS is approximately 0 Pa in the bulged regions. In the case of turbulent flows SST with a Reynolds number of 7500, the normalized WSS value tends to be 1Pa in all cases of aneurysm bulges. The steady-state study also examined variations in Reynolds number between 1150 and 7500 for each bulge ratio. Observations were made of the effects of laminar and turbulent conditions. Observations indicate that a ratio of 1.25 reduces pressure, and WSS changes to a comparable degree. Variations in WSS and pressure caused by aneurysms are normal for a smaller bulge ratio.

The inflation's wall shear stress (WSS) seen from the waveforms is minimal compared to the straight vessels' WSS.[35] The shear force on the intake wall is equivalent to that of Poiseuille flow, which occurs when the artery is not dilated. A convective slowdown of the flow in the proximal half of the tiny aneurysm results in highly minor velocity gradients at the wall, resulting in a near-zero magnitude wall shear stress.[48] Endothelial cells and normal physiology are negatively affected by low WSS. Low WSS also has a significant impact on the remodeling of artery walls, the formation of aneurysms, and the rupture of these vessels. Comparatively, the shear stress transport (SST) model performed well for bulge ratios ranging from = 1.25 to 2.5. Compared to the distal and proximal ends, the variance in the bulge region is observed to be the least. With bulge expansion, pressure rises slightly in the models depicted in Figs. 15a-e.

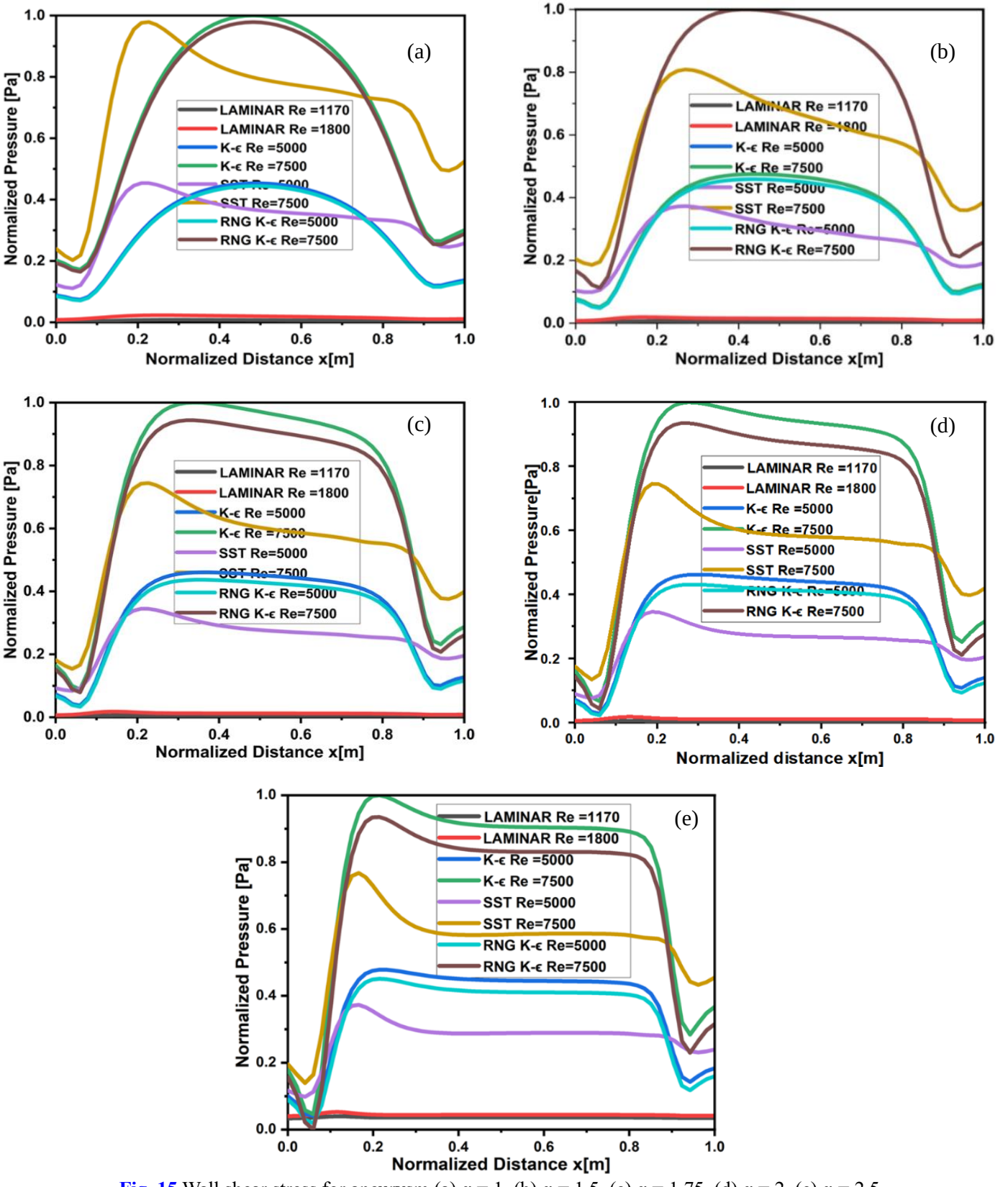

Fig. 15 Wall shear stress for aneurysm (a) α = 1, (b) α = 1.5, (c) α = 1.75, (d) α = 2, (e) α = 2.5.

Throughout the distal portion of the bulge, the pressure decreased. When the laminar flow was taken into account, the most significant pressure was found at the mid-point of the aneurysm bulge. In addition, the pressure at the output remained to some extent higher when the flow was laminar, although almost equal to the input pressure. The exit fell slightly below the input pressure when turbulent flow in disparity to the previous. Figs. 15a-e shows the pressure measurements for several increasing Reynolds values for various models. It has also been studied how the pressure drop

fluctuates with model size. The findings for diverse flow conditions are revealed for several flow rates: two with the smooth, laminar flow with Re = 1170 and 1800, one with the fully turbulent flow with Re = 5000, and one with Re = 7500. A proximal increase in pressure occurred for all flow rates at the bulge zone. With the model size, the pressure surge is proportional to the surge in bulge ratio up to D/d = 2.5. The overlap of the curves also shows that pressure increased regardless of whether the flow was laminar or turbulent. The most significant models were under the highest pressure at the bulge midpoint. The most considerable significant pressure was recorded near the aneurysm bulge's midway considering laminar flow. In addition, when the flow was laminar, the output pressure remained somewhat more significant, although being almost equal to the input pressure. The pressure analysis is a salient feature because it suggests that, for two different reasons, the largest in vivo aneurysms are exposed to maximum pressure forces. The law of Laplace[49] shows that, even if the fluid pressure remains constant, the magnitude of the WSS increases as the bulging diameter grows.

The fluid pressure, on the other hand, is not constant. Finally, the reduced diameter restricts the maximum pressure generated at the center of the bulge, as referred to in Figs. 15a-e. The reduced diameter also reduces the risk of rupture. It is also reported that WSS outcomes are significant physiologically since in vivo AAAs can be laminar or turbulent.[50] Full development of turbulence leads to an increase in the amount of shear stress on the distal end of the bulge model and causes even more immediate stress. The bulging wall's recirculating fluid movement is associated with a higher pressure at the center of the bulge than at the entrance. This pressure distribution is presumably due to a Bernoulli effect. As a result, its average speed decreases as the flow enters the bulge region. The same effect can be seen in real AAAs in case of turbulence, namely to augment the endothelial wall shear at the distal end of the aneurysm. As a result, there is an increase in the risk of damage to the bulge region. It can be concluded that larger models (larger aneurysm models) are turbulent at lower flow rates than smaller models. The most significant models are also subject to incredible stress on the peak wall shear. The flow's convective acceleration and deceleration and the viscous contact between the wall and the fluid determine the wall pressure patterns that are especially relevant.[48,51]

4. Conclusions

This paper presents numerical and computational results of steady-state flow through an abdominal aortic aneurysm. This work developed generic pipes with and without aneurysmal flow models, and their numerical and computational results are presented in this paper. A dimensionless Reynolds number characterizes the issue regarding the aneurysm by describing the dilation length, maximum diameter, and physical flow parameters. This value varies between 500 and 7500 to investigate the influence of laminar and turbulent flow in generic without aneurysm and aneurysmal aorta models. Generic without aneurysm aorta and five different aneurysmal aorta designs were studied to find their ability to initiate and propagate rupture.

Furthermore, differences in WSS, pressure, and velocity were examined in these models to determine how the rupture developed. The study investigated the numerical and computational results obtained for the generic aorta without an aneurysm model. According to the data seen from the tabulation, the velocity deviates by 0.7 percent from the projected value. The difference in pressure ΔP was 2%, whereas the difference in WSS was 4%. These findings related to 104800 analytical and theoretical mesh components.

Additionally, an aneurysmal aorta model reported a pressure differential variation of 2%. Compared to the analytical findings obtained using the equations and the CFD, the maximum velocity is comparable to the theoretical value for an aneurysmal aorta model with a 3% variation. Additionally, the pressure uncertainty derived from analytical and CFD data is 2% and can be allowed to be 10% due to smooth transitions and pipe expansion.

The graphical representation demonstrates that the WSS is negligible when the bulge size is small. The WSS increases in direct proportion to the bulge's size. This finding established that WSS has a considerable effect on the size of bulges. Thus, the search for WSS may be critical throughout the aneurysm's examination. Pressure fluctuations are also explored, providing insight into linking these parameters for clinical reference purposes. The geometry model for aneurysms is divided into patient-specific and general evaluation models. The former can acquire unique information before an operational situation, allowing for individual prediction of the current in a Vivo flow field. Generic models provide a broader representation of the problem, allowing for comparisons between diverse research groups, WSS estimators, and CFD codes. As a result, the current investigation used the abdominal aortic aneurysm generic geometry.

Conflict of Interest

The authors declare no conflict of interest.

Supporting information

Not applicable.

References

[1] R. Erbel, V. Aboyans, C. Boileau, E. Bossone, R. di Bartolomeo, H. Eggebrecht, A. Evangelista, V. Falk, H. Frank, O. Gaemperli, M. Grabenwöger, A. Haverich, B. Iung, A. Manolis, F. Meijboom, C. Nienaber, M. Roffi, H. Rousseau, U. Sechtem, P. A. Sirnes, R. Allmen, C. Vrints, *Kardiologia Polska*, 2014, **72**, 1169-1252, doi: 10.5603/kp.2014.0225.

[2] J. Carter, D. Morris, P. Sherliker, R. Clack, K. Lam, A. Halliday, R. Clarke, S. Lewington, R. Bulbulia, *Journal of the American Heart Association*, 2020, **9**, doi:

10.1161/jaha.119.014748.
[3] B. Liu, D. Granville, J. Golledge, Z. Kassiri, *American Journal of Physiology Heart and Circulatory Physiology*, 2020, **318**, 652-670, doi: 10.1152/ajpheart.00621.2019.
[4] S. Aggarwal, A. Qamar, V. Sharma, A. Sharma, Experimental & Clinical Cardiology, 2011, **16**, 11, PMID: 21523201.
[5] J. Gwon, T. Kwon, Y. Cho, Y. Han, M. Noh, *Annals of Surgical Treatment and Research*, 2016, **91**, 303, doi: 10.4174/astr.2016.91.6.303.
[6] H. Salman, B. Ramazanli, M. Yavuz, H. Yalcin, *Frontiers in Bioengineering and Biotechnology*, 2019, **7**, 111, doi: 10.3389/fbioe.2019.00111.
[7] B. Baxter, M. Terrin, R. Dalman, *Circulation*, 2008, **117**, 1883-1889, doi: 10.1161/circulationaha.107.735274.
[8] Y. Shimazaki, H. Ueda, *Cham: Springer International Publishing*, 2013, 161-179, doi: 10.1007/978-3-319-01074-8_8.
[9] N. Miguntanna, H. Moses, M. Sivakumar, S. Yang, K. Enever, M. Riaz, *Environmental Fluid Mechanics*, 2020, **20**, 953-986, doi: 10.1007/s10652-019-09733-6.
[10] G. Franck, J. Dai, A. Fifre, S. Ngo, C. Justine, S. Michineau, E. Allaire, M. Gervais, *Circulation*, 2013, **127**, 1877-1887, doi: 10.1161/circulationaha.113.001677.
[11] S. Haller, A. Azarbal, S. Rugonyi, *Bioengineering*, 2020, **7**, 79, doi: 10.3390/bioengineering7030079.
[12] G. Louridas, K. Reilly, M. Perry, *South African Medical Journal*, 1990, **78**, 642-643, PMID: 2251606.
[13] R. Budwig, D. Elger, H. Hooper, J. Slippy, *Journal of Biomechanical Engineering*, 1993, **115**, 418-423, doi: 10.1115/1.2895506.
[14] M. Fillinger, S. Marra, M. Raghavan, F. Kennedy, *Journal of Vascular Surgery*, 2003, **37**, 724-732, doi: 10.1067/mva.2003.213.
[15] M. Urquijo, R. Zamacona, A. Mendoza, M. Iribarren, E. Ibarra, M. Bencomo, M. Fabiani, *Vascular and Endovascular Surgery*, 2021, **55**, 677-683, doi: 10.1177/15385744211012926.
[16] E. Pérez, L. Solórzano, E. Finol, *Chemical Engineering Transactions*, 2016, **49**, 73-78, doi: 10.3303/CET1649013.
[17] R. Peattie, C. Asbury, E. Bluth, J. Ruberti, *Journal of Ultrasound in Medicine*, 1996, **15**, 679-688, doi: 10.7863/jum.1996.15.10.679.
[18] R. Peattie, C. Asbury, E. Bluth, T. Riehle, *Journal of Ultrasound in Medicine*, 1996, **15**, 689-696, doi: 10.7863/jum.1996.15.10.689.
[19] N. Kumar, S. Wahal, A. Ganesha, A. Murthy, *International Journal of Mechanical and Production Engineering Research and Development*, 2019, **65**, 733-742, doi: 10.24247/ijmperdoct201965.
[20] J. Nikuradse, National Advisory Committee for Aeronautics, *Laws of flow in rough pipes*, 1950.
[21] T. Bergman, A. Lavine, F. Incropera, D. DeWitt, *Introduction to heat transfer*. John Wiley & Sons, 2011.
[22] A. Yunus, *Fluid Mechanics: Fundamentals and Applications (Si Units)*. Tata McGraw Hill Education Private Limited, 2010.
[23] S. Umair, E. Ansari, A. Khan, S. Alrobaian, *CFD Letters*, 2019, **11**, 63-71.
[24] B. Staarmann, M. Smith, C. Prestigiacomo, *Neurosurgical Focus*, 2019, **47**, E2, doi: 10.3171/2019.4.focus19225.
[25] K. Khanafer, P. Gadhoke, R. Berguer, J. Bull, *Biorheology*, 2006, **43**, 661-79, PMID: 17047283.
[26] M. Wong, L. Sheng, C. Azwadi, G. Hashim, *International Journal of Advanced Research*, 2015, **6**, 34-48.
[27] F. White, *Fluid Mechanics 5th edition McGraw Hill Book Company. New York, USA*, 2003, 52-78.
[28] A. Bauer, M. Bopp, S. Jakirlic, C. Tropea, A. Krafft, N. Shokina, J. Hennig, *Experiments in Fluids*, 2020, **61**, 59, doi: 10.1007/s00348-020-2901-4.
[29] A. Impiombato, G. Civita, F. Orlandi, F. Franceschini Zinani, L. Rocha, C. Biserni, *Dynamics*, 2021, **1**, 9-17, doi: 10.3390/dynamics1010002.
[30] I. Ansys, ANSYS fluent user's guide, release 19.0, *ANSYS Inc, Canonsburg*, 2018.
[31] A. N. S. Y. S. CFX-Solver, Theory Guide, Release ll, *ANSYS Inc., Canonsburg*, 2006.
[32] B. Munson, D. Young, T. Okiishi, *Fundamentals of fluid mechanics. New York: Wiley*, 1994.
[33] A. Bauer, S. Wegt, M. Bopp, S. Jakirlic, C. Tropea, A. Krafft, N. Shokina, J. Hennig, G. Teschner, H. Egger, *Experiments in Fluids*, 2019, **60**, 112, doi: 10.1007/s00348-019-2758-6.
[34] G. Sheard, *Journal of Engineering Mathematics*, 2009, **64**, 379-390, doi: 10.1007/s10665-008-9261-z.
[35] S. S. Gopalakrishnan, B. Pier, A. Biesheuvel, *Journal of Fluid Mechanics*, 2014, **758**, 150-179, doi: 10.1017/jfm.2014.535.
[36] G. Fung, S. Lam, S. Cheng, K. Chow, *Computers in Biology and Medicine*, 2008, **38**, 484-9, doi: 10.1016/j.compbiomed.2008.01.012.
[37] S. Lam, G. Fung, S. Cheng, K. W. Chow, *29th Annual International Conference of the IEEE Engineering in Medicine and Biology Society*, 2007, 943-946, doi: 10.1109/IEMBS.2007.4352447.
[38] F. Gao, M. Watanabe, T. Matsuzawa, *BioMedical Engineering OnLine*, 2006, **5**, 25, doi: 10.1186/1475-925x-5-25.
[39] F. Gao, M. Watanabe, T. Matsuzawa, *Eighth International Conference on High-Performance Computing in Asia-Pacific Region, IEEE*, 2005, **9**, 169, doi: 10.1109/HPCASIA.2005.95.
[40] H. Versteeg, W. Malalasekera, An introduction to computational fluid dynamics: the finite volume method, *Pearson education*, 2007.
[41] J. Anderson, Computational Fluid Dynamics: Podstawy z aplikacjami, 1995.
[42] P. Constantin, C. Foias, Navier-stokes equations, *Navier-stokes equations. University of Chicago Press*, 2020.
[43] Y. Fung, *Biomechanics*. 1993, 321-391, doi: 10.1007/978-1-4757-2257-4_8.
[44] Y. A. Cengel, *Tata McGraw-Hill Education*, 2010.
[45] J. Štigler, *Engineering Mechanics*, 2014, **21**, 371-379.
[46] A. Javadzadegan, B. Fakhim, M. Behnia, M. Behnia, *European Journal of Mechanics-B/Fluids*, 2014, **46**, 109-117, doi: 10.1016/j.euromechflu.2014.02.011.
[47] D. Rennels, H. Hudson, Pipe Flow, *Pipe Flow. Hoboken, NJ: John Wiley & Sons, Inc.*, 2012.
[48] E. Finol, C. Amon, *Computer Methods in Biomechanics and*

Biomedical Engineering, 2002, **5**, 309-318, doi: 10.1080/1025584021000009742.
[49] T. Taylor, T. Yamaguchi, *Journal of Biomechanical Engineering*, 1994, **116**, 89-97, doi: 10.1115/1.2895709.
[50] E. Bluth, S. Murphey, L. Hollier, M. A. Sullivan, *International Angiology*, 1990, **9**, 8-10, PMID: 2212801.
[51] C. Stamatopoulos, Y. Papaharilaou, D. Mathioulakis, A. Katsamouris, *Experimental Thermal and Fluid Science*, 2010, **34**, 915-927, doi: 10.1016/j.expthermflusci.2010.02.008.

Author Information

Sunitha Lasrado *received her B.E. degree in Electronics and Communication Engineering and M.Tech. degree in Microelectronics and Control systems from Visvesvaraya Technological University, Belagavi, India. She is currently pursuing her Ph.D. degree with the Department of Electronics and Communication Engineering, Manipal Institute of Technology, Manipal Academy of Higher Education, Manipal, India. Her research interest includes Biomechanics, Computational Fluid Dynamics. She is a member of ISTE, ISEE, ISSE, India.*

S Balaji *is an Associate Professor and Head of the Department of Biotechnology, Manipal Institute of Technology, Manipal Academy of Higher Education. His research interests are bio-, nano- and chem-informatics and technologies, respectively. He has, published over 60 research papers in reputed journals and delivered several guest lectures. He is also a recipient of young scientist award for the year 2010–2011 from the Govt. of Karnataka, India.*

R Vinoth *is an Associate Professor of Electronics and Communication Engineering Department in Manipal Institute of Technology, Manipal, Karnataka, India. He obtained his Ph.D in the area of Computational Biomechanics at Periyar Maniammai University, Thanjavur, India. He received his Master of Technology in Biomedical Signal Processing and Instrumentation from SASTRA University, Thanjavur, India and Bachelor of Engineering in Electronics and Communication Engineering from NIT, Trichy, India. His research interest includes Power Electronics, Biomechanics and Medical Electronics. He has work experience of 23+ years and published 25 research papers.*